symmetry

MDPI

Article

Vibration Analysis of a Finite Lightweight Locally Resonant Beam Suspended with Periodic Force-Moment-Type Resonators inside Using an Exact Wave-Based Approach

Hangyuan Lv [1,2,*], Shangjie Li [1,2], Xianzhen Huang [1,2] and Zhongliang Yu [3]

[1] School of Mechanical Engineering and Automation, Northeastern University, Shenyang 110819, China; 1910123@stu.neu.edu.cn (S.L.); xzhhuang@mail.neu.edu.cn (X.H.)
[2] Key Laboratory of Vibration and Control of Aero Propulsion Systems Ministry of Education of China, Northeastern University, Shenyang 110819, China
[3] College of New Materials and New Energies, Shenzhen Technology University, Shenzhen 518118, China; yuzl@mail.neu.edu.cn
* Correspondence: lvhy@me.neu.edu.cn

Abstract: This paper employs and develops the exact wave-based vibration analysis approach to investigate the propagation properties of a designed finite lightweight locally resonant (LR) beam with two-degree-of-freedom (2-DOF) force-moment-type resonators attached periodically inside. By deriving the propagation, reflection, and transmission matrices of the structural discontinuities, the vibration of the LR beam can be described as structural waves. By assembling wave relations into the beam, the approach shows high efficiency because the forced vibration problem of the lightweight LR structure is turned to be the solution to a related set of matrix equations. The accuracy of the developed approach is validated with two examples carried out using the finite element method. In addition, the influence of the main parameters of the LR beam is studied and we found that the increase in the mass of the resonator and the stiffness of the spring are more sensitive in broadening the width and increasing the center frequency of the band gap of the designed lightweight LR beam. The proposed structure and analysis approach in this paper may provide an exact and efficient means for the design and analysis of structures in which damping and lightweight properties are required, such as space-arm and the framework of antennas in the field of aerospace.

Keywords: locally resonant beam; lightweight; vibration damping; wave-based vibration analysis

Citation: Lv, H.; Li, S.; Huang, X.; Yu, Z. Vibration Analysis of a Finite Lightweight Locally Resonant Beam Suspended with Periodic Force-Moment-Type Resonators inside Using an Exact Wave-Based Approach. *Symmetry* **2022**, *14*, 1542. https://doi.org/10.3390/sym14081542

Academic Editor: Lingling Wu

Received: 29 June 2022
Accepted: 25 July 2022
Published: 27 July 2022

1. Introduction

There has been growing interest in designing phononic crystals (PCs) and acoustics/elastic metamaterials (AMs/EMs) [1–3], mainly because these periodic structures can be designed to prevent the propagation of flexural waves. Based on this characteristic, the periodic structures have been widely applied in vibration and acoustic equipment. Among them, the excellent damping effect of locally resonant (LR) beams makes it very promising in engineering applications [4–6], in which the resonator is a continuous Timoshenko or Euler beam coupled with one or several spring-mass structures. Increasingly more researchers have recently studied the propagation properties of the flexural waves in specific frequency bounds along the LR beams, known as band gaps.

As a general structure for many engineering problems, analysis of the band gap properties of LR beams is of great significance. The most typical analysis methods include the transfer matrix method (TMM) [7,8], finite element method (FEM) [9–13], and spectral element method [14], and increasingly more new methods have been developed. The band gap properties of a Euler–Bernoulli beam with a four-link mechanism were studied in [15], where the band gap can be adjusted by the geometrical parameters of the four-link mechanism. The transition criterion was established in [16], where the trend of the LR beam

band structure changing with the spring constant or local resonator mass was analyzed by an improved TMM. The above studies realized the analysis and expansion of the band gaps of various periodic LR beams. Furthermore, lightweight LR beams are widely used in the aerospace field and analysis of their structures and band gap properties has become a hot research topic.

Recently, some lightweight LR beams and metamaterials have been constructed and studied for their band gap properties [17–19]. Tan et al. [17] proposed a reusable metamaterial for energy absorption, and it was verified through a combination of compression experiments and simulations that the proposed structure has larger specific energy absorption and higher energy absorption efficiency than that of most traditional negative stiffness structures. A lightweight LR beam was designed to increase the bending stiffness to improve the energy dissipation, and experiments under cyclic loading showed that the proposed structure exhibited sequential snap-through transitions with relatively large energy dissipation [18]. By utilizing prefabricated curved beams and rigid bracing frames, a range of multidirectional buckling-based metamaterials were proposed and analyzed in [19], and the analysis results show that the designed metamaterial has a stronger absorption ability for impact energy. A lightweight and unstable three-dimensional microlattice was designed in [20], which demonstrates very good repeatable and time-scale-independent energy dissipation, and Findeise et al. [21] carried out detailed analysis and numerical study on its dissipation mechanism and deformation, where the behavior of the internal structure was studied by analyzing the interaction between a periodic cell, a single buckling element, and multiple unstable elements. Ma et al. [22] designed a self-recoverable and reusable metamaterial via 3D printing and demonstrated through FEM and experiments that the newly designed metamaterial can effectively dissipate energy via elastic deformation. By adding an inclusion with a low natural resonance frequency into a hollow, cellular, polymer structure, a kind of lightweight LR beam is designed in Ref. [23] for low-frequency band gap, where the scattering matrix is obtained by measuring the velocities on both sides of the heterogeneous plate. Owing to these various remarkable characteristics, this structure can potentially be used to form structures that require both damping and lightweight properties, such as the space-arm and framework of antennas in the field of aerospace. Although some methods have been developed to analyze the energy adsorption capacity of these newly designed lightweight LR beams and metamaterials, the most commonly used FEM and experimental analysis are very time consuming.

To simplify the vibration analysis of LR beams, wave-based methods have been proposed and developed rapidly in recent years [24–28]. The transmission and reflection matrices for different discontinuities on a Timoshenko beam were first derived in [24], which greatly simplifies the wave-based vibration analysis method. Considering the joint influence of bending and longitudinal vibration on the classical planar frame structure, Mei et al. [29] proposed an analytical wave-based method to obtain its natural frequency. In [30], the wave-based method is employed to analyze the band gap properties of a finite Timoshenko beam carrying periodic two-degree-of-freedom uncoupled force-moment-type resonators, where the forced vibration problem is transformed into a problem of solving related matrix equations by assembling the wave relationships of the uncoupled force-moment-type resonator into the beam. The above studies demonstrated the high efficiency and wide applicability of the wave-based method.

In this paper, the wave-based methods are further developed and applied to study the band gap properties of a newly designed lightweight LR beam. In the LR beam, the 2-DOF force-moment-type resonators are attached inside periodically. With the wave-based analysis approach, the propagation, reflection, and transmission matrices at each discontinuity are derived and assembled as a module with MATLAB software. The design work for the lightweight LR beam is significantly simplified as the module can be called and modified easily through the modeling of the LR structure. The frequency response functions and band gap properties are obtained using both the wave-based approach and FEM to verify the efficiency and accuracy of the proposed analysis approach. Furthermore,

the influence of the main parameters of the LR beam on the band gap properties is studied. Finally, the increases in the mass of the resonator and the stiffness of the spring are validated to improve the width and increase the center frequency of the band gap through two examples. The purpose of this paper is to provide an advantageous means in the design and analysis of lightweight LR beams for vibration control in the situation of lightweight requirements, such as in the field of aerospace.

2. Wave-Based Analysis Methodology

2.1. Overview

The motion equations of bending, rotation, and longitudinal vibration of Timoshenko beams can be expressed as in [31]:

$$GA\kappa\left(\frac{\partial\psi(x,t)}{\partial x}-\frac{\partial^2 w(x,t)}{\partial x^2}\right)+\rho A\frac{\partial^2 w(x,t)}{\partial t^2}=q(x,t) \tag{1}$$

$$I\frac{\partial^2\psi(x,t)}{\partial x^2}+GA\kappa\left(\frac{\partial w(x,t)}{\partial x}-\psi(x,t)\right)-\rho I\frac{\partial^2\psi(x,t)}{\partial t^2}=0 \tag{2}$$

$$\rho A\frac{\partial^2 u(x,t)}{\partial t^2}-EA\frac{\partial^2 u(x,t)}{\partial x^2}=p(x,t) \tag{3}$$

where $\psi(x,t)$ indicates the rotation angle of the total bending section; x denotes the neutral axis position of the beam; t is time; $\partial w(x,t)/\partial x$ denotes the slope of the beam centerline; $w(x,t)$ and $u(x,t)$ represent the transverse deflection and longitudinal deflection, respectively; and the longitudinal and transverse forces applied on each unit length are expressed as $q(x,t)$ and $p(x,t)$, respectively. The shear coefficient κ, area moment of inertia I, and cross-sectional area A are the geometric properties. The shear modulus G, Young's modulus E, and mass density ρ are the material properties.

The shear force $V(x,t)$, bending moment $M(x,t)$, and longitudinal force $F(x,t)$ can be calculated as:

$$V(x,t)=GA\kappa\left(\frac{\partial w(x,t)}{\partial x}-\psi(x,t)\right) \tag{4}$$

$$M(x,t)=EI\frac{\partial\psi(x,t)}{\partial x} \tag{5}$$

$$F(x,t)=EA\frac{\partial u(x,t)}{\partial x} \tag{6}$$

Without considering the suppression time dependence $e^{i\omega t}$ and loading, the free-wave propagation Equations (1)–(3) can be calculated as:

$$w(x,t)=a_1^+e^{-ik_1x}+a_2^+e^{k_2x}+a_1^-e^{ik_1x}+a_2^-e^{k_2x} \tag{7}$$

$$\psi(x,t)=-iPa_1^+e^{-ik_1x}-Na_2^+e^{-k_2x}+iPa_1^-e^{ik_1x}+Na_2^-e^{k_2x} \tag{8}$$

$$u(x,t)=c^+e^{-ik_3x}+c^-e^{ik_3x} \tag{9}$$

where $k_1, k_2,\ k_3$ are three wavenumbers; the superscripts $-$ or $+$ indicate the backward or forward propagating waves; and c, a_1, and a_2 represent the amplitudes of the propagating longitudinal waves, propagating soft waves, and near-field soft waves, respectively. iP and N relate the rotational solution to the transverse displacement solution as:

$$P=k_1\left(1-\frac{\omega^2}{k_1^2C_s^2}\right),\quad N=k_2\left(1+\frac{\omega^2}{k_2^2C_s^2}\right) \tag{10}$$

The relationships about the wavenumber-frequency dispersion can be derived as follows:

$$k_1 = \sqrt{\frac{1}{2}\left[\left(\frac{1}{C_s}\right)^2 + \left(\frac{C_r}{C_b}\right)^2\right]\omega^2 + \sqrt{\left(\frac{\omega}{C_b}\right)^2 + \frac{1}{4}\left[\left(\frac{1}{C_s}\right)^2 - \left(\frac{C_r}{C_b}\right)^2\right]^2\omega^4}} \quad (11)$$

$$k_2 = \sqrt{-\frac{1}{2}\left[\left(\frac{1}{C_s}\right)^2 + \left(\frac{C_r}{C_b}\right)^2\right]\omega^2 + \sqrt{\left(\frac{\omega}{C_b}\right)^2 + \frac{1}{4}\left[\left(\frac{1}{C_s}\right)^2 - \left(\frac{C_r}{C_b}\right)^2\right]^2\omega^4}} \quad (12)$$

$$k_3 = \sqrt{\frac{E}{\rho}\omega^2} \quad (13)$$

in which the wave speeds for rotation, shear, and bending are defined as:

$$C_r = \sqrt{\frac{\rho I}{\rho A}}, C_b = \sqrt{\frac{EI}{\rho A}}, C_s = \sqrt{\frac{GA\kappa}{\rho A}} \quad (14)$$

2.2. Propagation Matrix

The exact wave propagation state in a single frequency along a uniform beam between discontinuities is expressed by Equations (7)–(9). Suppose points A and B fall between the discontinuities of a beam spaced at a distance x, which is shown in Figure 1. Since only bending vibration in the LR beam is considered, the propagation matrix is defined as:

$$\boldsymbol{b}^+ = \boldsymbol{f}(x)\boldsymbol{a}^+, \boldsymbol{a}^- = \boldsymbol{f}(x)\boldsymbol{b}^- \quad (15)$$

in which:

$$\boldsymbol{a}^+ = \begin{bmatrix} a_1^+ \\ a_2^+ \end{bmatrix}, \boldsymbol{a}^- = \begin{bmatrix} a_1^- \\ a_2^- \end{bmatrix}, \boldsymbol{b}^+ = \begin{bmatrix} b_1^+ \\ b_2^+ \end{bmatrix}, \boldsymbol{b}^- = \begin{bmatrix} b_1^- \\ b_2^- \end{bmatrix} \quad (16)$$

where $\boldsymbol{a}^+$ and $\boldsymbol{b}^+$ represent the forward propagating wave coefficients at points A and B, respectively. $\boldsymbol{a}^-$ and $\boldsymbol{b}^-$ are the backward propagating wave coefficients at points A and B, respectively:

$$\boldsymbol{f}(x) = \begin{bmatrix} e^{-ik_1 x} & 0 \\ 0 & e^{-k_2 x} \end{bmatrix} \quad (17)$$

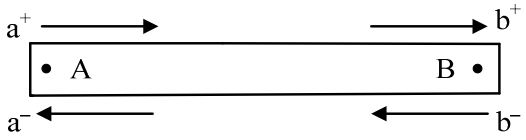

Figure 1. Wave propagation between two points of a uniform beam at a distance of x.

2.3. Reflection at a Free Boundary

This paper studies the LR beam with a free endless boundary without considering transverse forces and bending moments. A reflection matrix can be established to represent the relationship between the reflected waves $\boldsymbol{a}^-$ and incident waves $\boldsymbol{a}^+$ as:

$$\boldsymbol{a}^- = \boldsymbol{r}_f \boldsymbol{a}^+ \quad (18)$$

where:

$$\boldsymbol{r}_f = \begin{bmatrix} \frac{-Pk_1(-N+k_2)+ik_2N(k_1-P)}{Pk_1(-N+k_2)+ik_2N(k_1-P)} & \frac{2Nk_2(-N+k_2)}{Pk_1(-N+k_2)+ik_2N(k_1-P)} \\ \frac{2iPk_1(-P+k_1)}{Pk_1(-N+k_2)+ik_2N(k_1-P)} & \frac{Pk_1(-N+k_2)-ik_2N(k_1-P)}{Pk_1(-N+k_2)+ik_2N(k_1-P)} \end{bmatrix} \quad (19)$$

2.4. Applied Forces and Moments

The waves $\boldsymbol{a}$ and $\boldsymbol{b}$ generated by the external force $\boldsymbol{F}$ at $x = 0$ are drawn in Figure 2, and the conditions of equilibrium and continuity can be given as:

$$\boldsymbol{b}^{+} - \boldsymbol{a}^{+} = \boldsymbol{f} \tag{20}$$

$$\boldsymbol{b}^{-} - \boldsymbol{a}^{-} = -\boldsymbol{f} \tag{21}$$

where the amplitude vector of the excited wave is given:

$$\boldsymbol{f} = \begin{bmatrix} iN \\ P \end{bmatrix} \frac{F}{GA\kappa(k_2 P - k_1 N)} \tag{22}$$

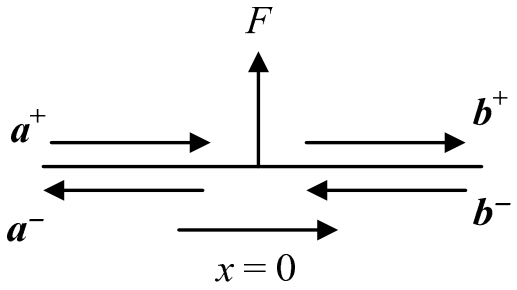

Figure 2. Waves generated by external force.

2.5. Transmission and Reflection at the 2-DOF Force-Moment-Type Resonator Attached Point

The LR beam suspended with force-moment-type resonators is shown in Figure 3, in which m is the mass of the resonator, k is the stiffness of the linear elastic spring, a is the length of the moment arm, and L is the lattice constant (distance between two adjacent resonators) of the LR beam.

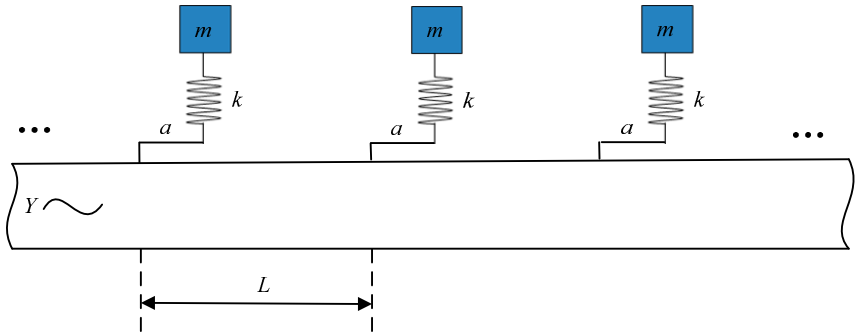

Figure 3. A beam with periodic 2-DOF force-moment-type resonators.

The resonator is the 2-DOF type because it applies force and moment to the host beam simultaneously, as depicted in Figure 4. In the figure, w_m is the transverse deflections of the mass blocks m. F is the force caused by the spring. w, u, and ψ are the transverse deflection, axial deflection, and angular rotation of the host beam at the point the resonator is attached. F and M are the force and moment of the resonator applied on the host beam, respectively. Note that the axial deflection u is not involved here because the 2-DOF force-moment-type resonator does not apply axial force to the host beam.

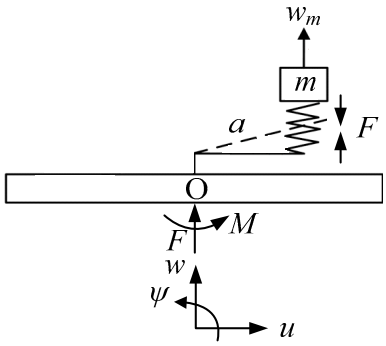

Figure 4. Free body diagram of a cell of resonators.

According to Figure 4, the equation of motion of the resonator can be expressed as:

$$-F = m\ddot{w}_m \tag{23}$$

where:

$$F = k(w_m - w + a\psi) \tag{24}$$

Considering the motion of the system is time harmonic with the frequency ω, by combining Equations (23) and (24), the displacements of the mass block w_m can be expressed in terms of the deflection at the attachment point w as:

$$w_m = \frac{k}{k - m\omega^2}(w + a\psi) \tag{25}$$

Then, the force F and the moment M applied by the resonator to the host beam can be obtained from Equations (24) and (25):

$$F = r{\cdot}(w + a\psi) \tag{26}$$

$$M = F{\cdot}a = r{\cdot}a(w + a\psi) \tag{27}$$

where:

$$r = \frac{km\omega^2}{k - m\omega^2}$$

As in [30], the applied force and moment generated by the resonators can be considered as injecting waves into the host beam. Combining Equations (7)–(9), (20) and (21), and substituting the expressions of the transverse force F and bending moment M in Equations (26) and (27) into Equation (22), the relations of the vibration waves at the point the resonator is attached can be obtained as:

$$\begin{bmatrix} \boldsymbol{A_{p1}} & \boldsymbol{A_{n1}} \\ \boldsymbol{A_{p2}} & \boldsymbol{A_{n2}} \end{bmatrix} \begin{bmatrix} \boldsymbol{a}^+ \\ \boldsymbol{a}^- \end{bmatrix} + \begin{bmatrix} \boldsymbol{B_{p1}} & \boldsymbol{B_{n1}} \\ \boldsymbol{B_{p2}} & \boldsymbol{B_{n2}} \end{bmatrix} \begin{bmatrix} \boldsymbol{b}^+ \\ \boldsymbol{b}^- \end{bmatrix} = 0 \tag{28}$$

where the coefficient matrices in Equation (28) are:

$$\boldsymbol{A_{p1}} = \begin{bmatrix} ira^2P\beta_2 + raNP\beta_1 - ra\beta_2 + irN\beta_1 + 1 & -iraN^2\beta_1 - ra\beta_2 + irN\beta_1 + ra^2N\beta_2 \\ P\beta_1 r + ra\beta_2 - iraP^2\beta_1 - ira^2P\beta_2 & rP\beta_1 - raNP\beta_1 + ra\beta_2 - ra^2N\beta_2 + 1 \end{bmatrix}$$

$$\boldsymbol{A_{p2}} = \begin{bmatrix} ira^2P\beta_2 - raNP\beta_1 - ra\beta_2 - irN\beta_1 & iraN^2\beta_1 - ra\beta_2 - irN\beta_1 + ra^2N\beta_2 \\ -P\beta_1 r + ra\beta_2 + iraP^2\beta_1 - ira^2P\beta_2 & -rP\beta_1 + raNP\beta_1 + ra\beta_2 - ra^2N\beta_2 \end{bmatrix}$$

$$\boldsymbol{A_{n1}} = \begin{bmatrix} -ira^2P\beta_2 + irN\beta_1 - raNP\beta_1 - ra\beta_2 & irN\beta_1 + iraN^2\beta_1 - ra\beta_2 - ra^2N\beta_2 \\ rP\beta_1 + iraP^2\beta_1 + ira^2P\beta_2 + ra\beta_2 & rP\beta_1 + raNP\beta_1 + ra\beta_2 + ra^2N\beta_2 \end{bmatrix}$$

$$\boldsymbol{A_{n2}} = \begin{bmatrix} -ira^2P\beta_2 - irN\beta_1 + raNP\beta_1 - ra\beta_2 + 1 & -irN\beta_1 - iraN^2\beta_1 - ra\beta_2 - ra^2N\beta_2 \\ -rP\beta_1 - iraP^2\beta_1 + ira^2P\beta_2 + ra\beta_2 & -rP\beta_1 - raNP\beta_1 + ra\beta_2 + ra^2N\beta_2 + 1 \end{bmatrix}$$

$$\boldsymbol{B_{p1}} = \boldsymbol{B_{n2}} = \begin{bmatrix} -1 & 0 \\ 0 & -1 \end{bmatrix}$$

$$\boldsymbol{B_{p2}} = \boldsymbol{B_{n1}} = \begin{bmatrix} 0 & 0 \\ 0 & 0 \end{bmatrix}$$

$$\beta_1 = \frac{1}{2(GA\kappa)(k_2P - k_1N)}$$

$$\beta_2 = \frac{1}{2(EI)(k_1P + k_2N)}$$

2.6. Transmission and Reflection at the Point Section Change

For the beam with section change, we denote the incident and transmitted parameters with the subscripts L and R, respectively. The equations of motion depicted in Figure 5 are:

$$V_L = V_R \tag{29}$$

$$M_L = M_R \tag{30}$$

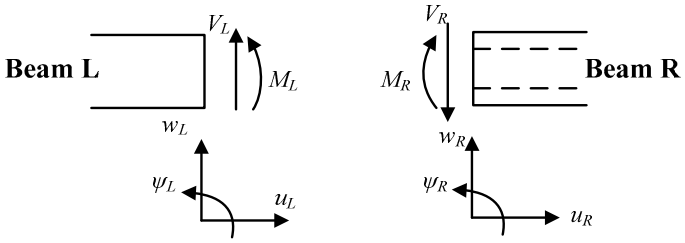

Figure 5. Free body diagram of a beam with a section changed.

The continuity conditions for the point section change are:

$$w_L = w_R \tag{31}$$

$$\psi_L = \psi_R \tag{32}$$

where the shear force and bending moment in Equations (29) and (30) are expressed as:

$$V_L = (GA\kappa)_L\left(\frac{\partial w_L}{\partial x_L} - \psi_L\right),\ V_R = (GA\kappa)_R\left(\frac{\partial w_R}{\partial x_R} - \psi_R\right) \tag{33}$$

$$M_L = (EI)_L\frac{\partial \psi_L}{\partial x_L},\ M_R = (EI)_R\frac{\partial \psi_R}{\partial x_R} \tag{34}$$

Assumed that two beams with different sections are joined at $x = 0$, as depicted in Figure 6. The incident waves $\boldsymbol{b}^{+}$ generate reflected waves $\boldsymbol{b}^{-}$ and transmitted waves $\boldsymbol{e}^{+}$, which are related to the incident waves through the reflection and transmission matrices by:

$$\boldsymbol{b}^{-} = \boldsymbol{r}_{LL}\,\boldsymbol{b}^{+}, \boldsymbol{e}^{+} = \boldsymbol{t}_{LR}\,\boldsymbol{b}^{+} \tag{35}$$

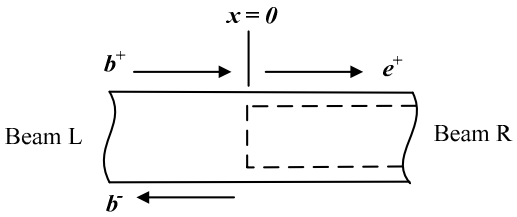

Figure 6. Reflection and transmission waves at the change in the section.

Considering Equations (29)–(35) can be put into a matrix form in terms of the reflection and transmission matrices $\boldsymbol{r}_{LL}$ and $\boldsymbol{t}_{LR}$, one has:

$$\begin{bmatrix} 1 & 1 \\ iP_L & N_L \end{bmatrix} \mathbf{r}_{LL} + \begin{bmatrix} -1 & -1 \\ iP_R & N_R \end{bmatrix} \mathbf{t}_{LR} = \begin{bmatrix} -1 & -1 \\ iP_L & N_L \end{bmatrix} \tag{36}$$

$$\boldsymbol{E}_{rLL}\mathbf{r}_{LL} + \boldsymbol{E}_{tLR}\mathbf{t}_{LR} = \boldsymbol{E}_{\mathbf{1}} \tag{37}$$

where:

$$\boldsymbol{E}_{r11} = \begin{bmatrix} (GA\kappa)_L(ik_{L1} - iP_L) & (GA\kappa)_L(k_{L2} - N_L) \\ -(EI)_L{\cdot}k_{L1}{\cdot}P_L & (EI)_L{\cdot}k_{L2}{\cdot}N_L \end{bmatrix}$$

$$\boldsymbol{E}_{t12} = \begin{bmatrix} -(GA\kappa)_R(-ik_{R1} + iP_R) & -(GA\kappa)_R(-k_{R2} + N_R) \\ (EI)_R{\cdot}k_{R1}{\cdot}P_R & -(EI)_R{\cdot}k_{R2}{\cdot}N_R \end{bmatrix}$$

$$\boldsymbol{E}_{\mathbf{1}} = \begin{bmatrix} -(GA\kappa)_L(-ik_{L1} + iP_L) & -(GA\kappa)_L(-k_{L2} + N_L) \\ (EI)_L{\cdot}k_{L1}{\cdot}P_L & -(EI)_L{\cdot}k_{L2}{\cdot}N_L \end{bmatrix}$$

The reflection and transmission matrices $\mathbf{r}_{LL}$ and $\mathbf{t}_{LR}$ can be obtained by solving Equations (36) and (37).

3. Vibration Analysis with the Wave-Based Approach

Figure 7 denotes the designed lightweight LR beam suspended periodically with eight 2-DOF force-moment-type resonators inside. The physical parameters are marked in the figure. In each cell, the length of the hollow beam is L_1 and the length of the solid beam is L_2. Based on the approach described above, the designed beam can be considered as shown in Figure 8. Note that the distance d between the point resonator attached and the point section changed is defined as a very small number to match the model in Figure 7.

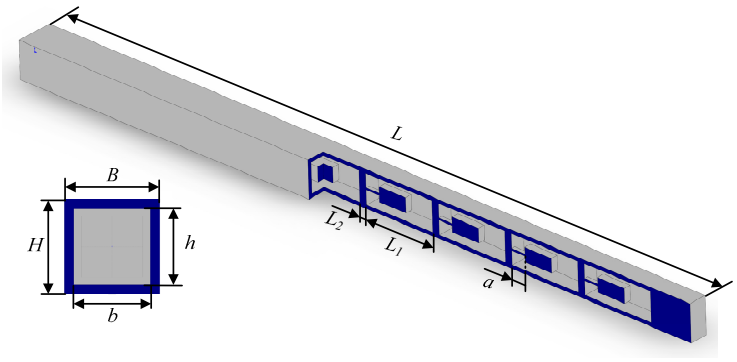

Figure 7. Model of the designed lightweight LR beam.

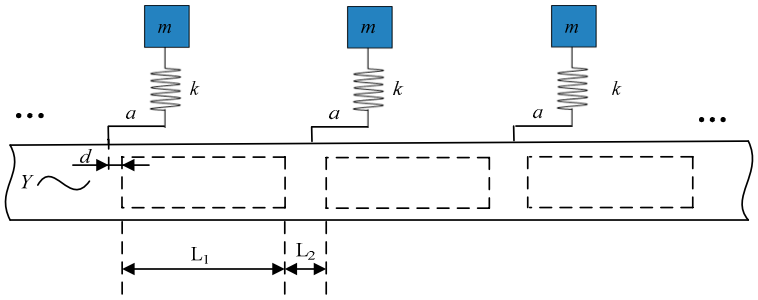

Figure 8. Equivalent model of the proposed LR beam for the wave-based approach.

Figure 9 illustrates the vibration wave components in the LR beam. As shown in the figure, the force-moment resonators are attached at points R_1, R_2, R_3, R_4, R_5, R_6, R_7, and R_8. The section-change points are labeled as B_1, B_2, B_3, B_4, B_5, B_6, B_7, and B_8 (section changes from a solid beam to a hollow beam), and C_1, C_2, C_3, C_4, C_5, C_6, C_7, and C_8 (section changes from a hollow beam to a solid beam). The boundary condition of the LR beam is free. The external force is applied at point G, and the insert force generates waves g_{11}^{+}, g_{11}^{-}, g_{12}^{+}, and g_{12}^{-}. The distance between the point G and the left end of the host beam (point A) is L_{11}, and the distance from point G to point R_1 (the first resonator attached point) is L_{12}. The length from the end of the last hollow beam to the right end of the host beam (point D) is L. Based on the propagation, transmission, and reflection relations described in Section 2, the relations of waves at discontinuities of the LR beam can be obtained as follows.

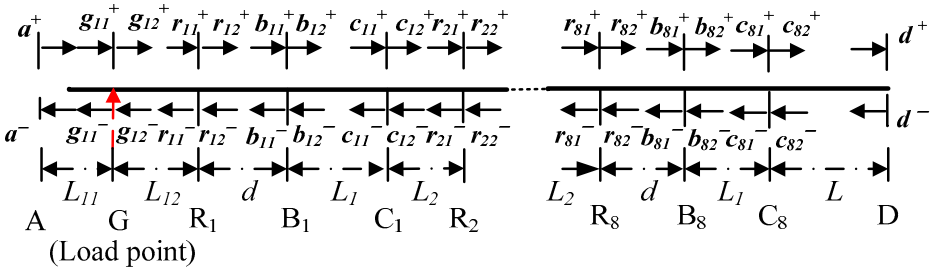

Figure 9. Vibration wave components in the LR beam.

At the eight resonator attachment points R_1, R_2, R_3, R_4, R_5, R_6, R_7, and R_8:

$$\begin{bmatrix} A_{p1} & A_{n1} \\ A_{p2} & A_{n2} \end{bmatrix} \begin{bmatrix} r_{11}^{+} \\ r_{11}^{-} \end{bmatrix} + \begin{bmatrix} B_{p1} & B_{n1} \\ B_{p2} & B_{n2} \end{bmatrix} \begin{bmatrix} r_{12}^{+} \\ r_{12}^{-} \end{bmatrix} = 0 \tag{38}$$

$$\begin{bmatrix} A_{p1} & A_{n1} \\ A_{p2} & A_{n2} \end{bmatrix} \begin{bmatrix} r_{21}^{+} \\ r_{21}^{-} \end{bmatrix} + \begin{bmatrix} B_{p1} & B_{n1} \\ B_{p2} & B_{n2} \end{bmatrix} \begin{bmatrix} r_{22}^{+} \\ r_{22}^{-} \end{bmatrix} = 0 \tag{39}$$

$$\begin{bmatrix} A_{p1} & A_{n1} \\ A_{p2} & A_{n2} \end{bmatrix} \begin{bmatrix} r_{31}^{+} \\ r_{31}^{-} \end{bmatrix} + \begin{bmatrix} B_{p1} & B_{n1} \\ B_{p2} & B_{n2} \end{bmatrix} \begin{bmatrix} r_{32}^{+} \\ r_{32}^{-} \end{bmatrix} = 0 \tag{40}$$

$$\begin{bmatrix} A_{p1} & A_{n1} \\ A_{p2} & A_{n2} \end{bmatrix} \begin{bmatrix} r_{41}^{+} \\ r_{41}^{-} \end{bmatrix} + \begin{bmatrix} B_{p1} & B_{n1} \\ B_{p2} & B_{n2} \end{bmatrix} \begin{bmatrix} r_{42}^{+} \\ r_{42}^{-} \end{bmatrix} = 0 \tag{41}$$

$$\begin{bmatrix} A_{p1} & A_{n1} \\ A_{p2} & A_{n2} \end{bmatrix} \begin{bmatrix} r_{51}^{+} \\ r_{51}^{-} \end{bmatrix} + \begin{bmatrix} B_{p1} & B_{n1} \\ B_{p2} & B_{n2} \end{bmatrix} \begin{bmatrix} r_{52}^{+} \\ r_{52}^{-} \end{bmatrix} = 0 \tag{42}$$

$$\begin{bmatrix} A_{p1} & A_{n1} \\ A_{p2} & A_{n2} \end{bmatrix} \begin{bmatrix} r_{61}^{+} \\ r_{61}^{-} \end{bmatrix} + \begin{bmatrix} B_{p1} & B_{n1} \\ B_{p2} & B_{n2} \end{bmatrix} \begin{bmatrix} r_{62}^{+} \\ r_{62}^{-} \end{bmatrix} = 0 \tag{43}$$

$$\begin{bmatrix} A_{p1} & A_{n1} \\ A_{p2} & A_{n2} \end{bmatrix} \begin{bmatrix} r_{71}^{+} \\ r_{71}^{-} \end{bmatrix} + \begin{bmatrix} B_{p1} & B_{n1} \\ B_{p2} & B_{n2} \end{bmatrix} \begin{bmatrix} r_{72}^{+} \\ r_{72}^{-} \end{bmatrix} = 0 \tag{44}$$

$$\begin{bmatrix} A_{p1} & A_{n1} \\ A_{p2} & A_{n2} \end{bmatrix} \begin{bmatrix} r_{81}{}^{+} \\ r_{81}{}^{-} \end{bmatrix} + \begin{bmatrix} B_{p1} & B_{n1} \\ B_{p2} & B_{n2} \end{bmatrix} \begin{bmatrix} r_{82}{}^{+} \\ r_{82}{}^{-} \end{bmatrix} = 0 \tag{45}$$

We use r_{ss} and t_{sh} to present the reflection and transmission matrices at the point the section changes from a solid beam to a hollow beam. Similarly, r_{hh} and t_{hs} present the reflection and transmission matrices at the point the section changes from a hollow beam to a solid beam. Thus, at the points the section changes from a solid beam to a hollow beam B_1:

$$b_{12}^{+} = t_{sh} b_{11}^{+} + r_{hh} b_{12}^{-} \tag{46}$$

$$b_{11}^{-} = r_{ss} b_{11}^{+} + t_{hs} b_{12}^{-} \tag{47}$$

At point B_2:

$$b_{22}^{+} = t_{sh} b_{21}^{+} + r_{hh} b_{22}^{-} \tag{48}$$

$$b_{21}^{-} = r_{ss} b_{21}^{+} + t_{hs} b_{22}^{-} \tag{49}$$

At point B_3:

$$b_{32}^{+} = t_{sh} b_{31}^{+} + r_{hh} b_{32}^{-} \tag{50}$$

$$b_{31}^{-} = r_{ss} b_{31}^{+} + t_{hs} b_{32}^{-} \tag{51}$$

At point B_4:

$$b_{42}^{+} = t_{sh} b_{41}^{+} + r_{hh} b_{42}^{-} \tag{52}$$

$$b_{41}^{-} = r_{ss} b_{41}^{+} + t_{hs} b_{42}^{-} \tag{53}$$

At point B_5:

$$b_{52}^{+} = t_{sh} b_{51}^{+} + r_{hh} b_{52}^{-} \tag{54}$$

$$b_{51}^{-} = r_{ss} b_{51}^{+} + t_{hs} b_{52}^{-} \tag{55}$$

At point B_6:

$$b_{62}^{+} = t_{sh} b_{61}^{+} + r_{hh} b_{62}^{-} \tag{56}$$

$$b_{61}^{-} = r_{ss} b_{61}^{+} + t_{hs} b_{62}^{-} \tag{57}$$

At point B_7:

$$b_{72}^{+} = t_{sh} b_{71}^{+} + r_{hh} b_{72}^{-} \tag{58}$$

$$b_{71}^{-} = r_{ss} b_{71}^{+} + t_{hs} b_{72}^{-} \tag{59}$$

At point B_8:

$$b_{82}^{+} = t_{sh} b_{81}^{+} + r_{hh} b_{82}^{-} \tag{60}$$

$$b_{81}^{-} = r_{ss} b_{81}^{+} + t_{hs} b_{82}^{-} \tag{61}$$

At the points the section changes from a hollow beam to a solid beam C_1:

$$c_{12}^{+} = t_{hs} c_{11}^{+} + r_{ss} c_{12}^{-} \tag{62}$$

$$c_{11}^{-} = r_{hh} c_{11}^{+} + t_{sh} c_{12}^{-} \tag{63}$$

At point C_2:

$$c_{22}^{+} = t_{hs} c_{21}^{+} + r_{ss} c_{22}^{-} \tag{64}$$

$$c_{21}^{-} = r_{hh} c_{21}^{+} + t_{sh} c_{22}^{-} \tag{65}$$

At point C_3:

$$c_{32}^{+} = t_{hs} c_{31}^{+} + r_{ss} c_{32}^{-} \tag{66}$$

$$c_{31}^{-} = r_{hh} c_{31}^{+} + t_{sh} c_{32}^{-} \tag{67}$$

At point C_4:

$$c_{42}^{+} = t_{hs} c_{41}^{+} + r_{ss} c_{42}^{-} \tag{68}$$

$$c_{41}^{-} = r_{hh}c_{41}^{+} + t_{sh}c_{42}^{-} \tag{69}$$

At point C_5:

$$c_{52}^{+} = t_{hs}c_{51}^{+} + r_{ss}c_{52}^{-} \tag{70}$$

$$c_{51}^{-} = r_{hh}c_{51}^{+} + t_{sh}c_{52}^{-} \tag{71}$$

At point C_6:

$$c_{62}^{+} = t_{hs}c_{61}^{+} + r_{ss}c_{62}^{-} \tag{72}$$

$$c_{61}^{-} = r_{hh}c_{61}^{+} + t_{sh}c_{62}^{-} \tag{73}$$

At point C_7:

$$c_{72}^{+} = t_{hs}c_{71}^{+} + r_{ss}c_{72}^{-} \tag{74}$$

$$c_{71}^{-} = r_{hh}c_{71}^{+} + t_{sh}c_{72}^{-} \tag{75}$$

At point C_8:

$$c_{82}^{+} = t_{hs}c_{81}^{+} + r_{ss}c_{82}^{-} \tag{76}$$

$$c_{81}^{-} = r_{hh}c_{81}^{+} + t_{sh}c_{82}^{-} \tag{77}$$

At the free support boundaries A and D:

$$a^{+} = r_f a^{-} \tag{78}$$

$$d^{-} = r_f d^{+} \tag{79}$$

In total, 26 pairs of propagation relations along the beam elements are included for the LR structure: AG, GR_1, R_1B_1, B_1C_1, C_1R_2, R_2B_2, B_2C_2, C_2R_3, R_3B_3, B_3C_3, C_3R_4, R_4B_4, B_4C_4, C_4R_5, R_5B_5, B_5C_5, C_5R_6, R_6B_6, B_6C_6, C_6R_7, R_7B_7. B_7C_7, C_7R_8, R_8B_8, B_8C_8, and C_8D. In the equations, f_s and f_h denote the propagation matrices along the solid and hollow beam, respectively:

Along AG:

$$g_{11}^{+} = f_s(L_{11})a^{+}, \quad a^{-} = f_s(L_{11})g_{11}^{-} \tag{80}$$

Along GR_1:

$$r_{11}^{+} = f_s(L_{12})g_{12}^{+}, \quad g_{12}^{-} = f_s(L_{12})r_{11}^{-} \tag{81}$$

Along R_1B_1:

$$b_{11}^{+} = f_s(d)r_{12}^{+}, \ r_{12}^{-} = f_s(d)b_{11}^{-} \tag{82}$$

Along B_1C_1:

$$c_{11}^{+} = f_h(L_1)b_{12}^{+}, \ b_{12}^{-} = f_h(L_1)c_{11}^{-} \tag{83}$$

Along C_1R_2:

$$r_{21}^{+} = f_s(L_2)c_{12}^{+}, \ c_{12}^{-} = f_s(L_2)r_{21}^{-} \tag{84}$$

Along R_2B_2:

$$b_{21}^{+} = f_s(d)r_{22}^{+}, \ r_{22}^{-} = f_s(d)b_{21}^{-} \tag{85}$$

Along B_2C_2:

$$c_{21}^{+} = f_h(L_1)b_{22}^{+}, \ b_{22}^{-} = f_h(L_1)c_{21}^{-} \tag{86}$$

Along C_2R_3:

$$r_{31}^{+} = f_s(L_2)c_{22}^{+}, \ c_{22}^{-} = f_s(L_2)r_{31}^{-} \tag{87}$$

Along R_3B_3:

$$b_{31}^{+} = f_s(d)r_{32}^{+}, \ r_{32}^{-} = f_s(d)b_{31}^{-} \tag{88}$$

Along B_3C_3:

$$c_{31}^{+} = f_h(L_1)b_{32}^{+}, \ b_{32}^{-} = f_h(L_1)c_{31}^{-} \tag{89}$$

Along C_3R_4:

$$r_{41}^{+} = f_s(L_2)c_{32}^{+}, \ c_{32}^{-} = f_s(L_2)r_{41}^{-} \tag{90}$$

Along R_4B_4:

$$\boldsymbol{b}_{41}^{+} = f_s(d)\boldsymbol{r}_{42}^{+}, \ \boldsymbol{r}_{42}^{-} = f_s(d)\boldsymbol{b}_{41}^{-} \tag{91}$$

Along B_4C_4:

$$\boldsymbol{c}_{41}^{+} = f_h(L_1)\boldsymbol{b}_{42}^{+}, \ \boldsymbol{b}_{42}^{-} = f_h(L_1)\boldsymbol{c}_{41}^{-} \tag{92}$$

Along C_4R_5:

$$\boldsymbol{r}_{51}^{+} = f_s(L_2)\boldsymbol{c}_{42}^{+}, \ \boldsymbol{c}_{42}^{-} = f_s(L_2)\boldsymbol{r}_{51}^{-} \tag{93}$$

Along R_5B_5:

$$\boldsymbol{b}_{51}^{+} = f_s(d)\boldsymbol{r}_{52}^{+}, \ \boldsymbol{r}_{52}^{-} = f_s(d)\boldsymbol{b}_{51}^{-} \tag{94}$$

Along B_5C_5:

$$\boldsymbol{c}_{51}^{+} = f_h(L_1)\boldsymbol{b}_{52}^{+}, \ \boldsymbol{b}_{52}^{-} = f_h(L_1)\boldsymbol{c}_{51}^{-} \tag{95}$$

Along C_5R_6:

$$\boldsymbol{r}_{61}^{+} = f_s(L_2)\boldsymbol{c}_{52}^{+}, \ \boldsymbol{c}_{52}^{-} = f_s(L_2)\boldsymbol{r}_{61}^{-} \tag{96}$$

Along R_6B_6:

$$\boldsymbol{b}_{61}^{+} = f_s(d)\boldsymbol{r}_{62}^{+}, \ \boldsymbol{r}_{62}^{-} = f_s(d)\boldsymbol{b}_{61}^{-} \tag{97}$$

Along B_6C_6:

$$\boldsymbol{c}_{61}^{+} = f_h(L_1)\boldsymbol{b}_{62}^{+}, \ \boldsymbol{b}_{62}^{-} = f_h(L_1)\boldsymbol{c}_{61}^{-} \tag{98}$$

Along C_6R_7:

$$\boldsymbol{r}_{71}^{+} = f_s(L_2)\boldsymbol{c}_{62}^{+}, \ \boldsymbol{c}_{62}^{-} = f_s(L_2)\boldsymbol{r}_{71}^{-} \tag{99}$$

Along R_7B_7:

$$\boldsymbol{b}_{71}^{+} = f_s(d)\boldsymbol{r}_{72}^{+}, \ \boldsymbol{r}_{72}^{-} = f_s(d)\boldsymbol{b}_{71}^{-} \tag{100}$$

Along B_7C_7:

$$\boldsymbol{c}_{71}^{+} = f_h(L_1)\boldsymbol{b}_{72}^{+}, \ \boldsymbol{b}_{72}^{-} = f_h(L_1)\boldsymbol{c}_{71}^{-} \tag{101}$$

Along C_7R_8:

$$\boldsymbol{r}_{81}^{+} = f_s(L_2)\boldsymbol{c}_{72}^{+}, \ \boldsymbol{c}_{72}^{-} = f_s(L_2)\boldsymbol{r}_{81}^{-} \tag{102}$$

Along R_8B_8:

$$\boldsymbol{b}_{81}^{+} = f_s(d)\boldsymbol{r}_{82}^{+}, \ \boldsymbol{r}_{82}^{-} = f_s(d)\boldsymbol{b}_{81}^{-} \tag{103}$$

Along B_8C_8:

$$\boldsymbol{c}_{81}^{+} = f_h(L_1)\boldsymbol{b}_{82}^{+}, \ \boldsymbol{b}_{82}^{-} = f_h(L_1)\boldsymbol{c}_{81}^{-} \tag{104}$$

Along C_8D:

$$\boldsymbol{d}^{+} = f_s(L)\boldsymbol{c}_{82}^{+}, \ \boldsymbol{c}_{82}^{-} = f_s(L)\boldsymbol{d}^{-} \tag{105}$$

The relations between the external force and the generated wave amplitudes are:

$$\boldsymbol{g}_{12}^{+} - \boldsymbol{g}_{11}^{+} = \boldsymbol{q} \tag{106}$$

$$\boldsymbol{g}_{12}^{-} - \boldsymbol{g}_{11}^{-} = -\boldsymbol{q} \tag{107}$$

Combining Equations (38)–(107) and putting it into matrix algebraic form gives:

$$\boldsymbol{A}_f \boldsymbol{z}_f = \boldsymbol{F} \tag{108}$$

where $\boldsymbol{A}_f$ is a 208×208 coefficient matrix, $\boldsymbol{z}_f$ is a 208×1 component vector, and $\boldsymbol{F}$ is a 208×1 vector holding the external transverse forces to the host beam.

4. Numerical Results and Discussion

It is considered that the material of the designed LR beam, as shown in Figure 7, is resin as an example. Some relevant parameters are as follows: the Poisson's ratio $v = 0.23$, the Young's modulus $E = 2.46$ GN/m^2, and the mass density $\rho = 1100$ kg/m^3. The shear coefficient is calculated by $\kappa = 10(1+v)/(12+11v)$, and the shear modulus can be

obtained from $G = \mathrm{E}/2(1+v)$ [32]. The width B and height H of the solid beam are both 25 mm, respectively. The inside width b and height h of the hollow beam are both 20 mm. The external excitation is applied at the position L_{11} = 8 mm from the left end of the host beam, and L_{12} = 22 mm. Meanwhile, the measured point is located at the point with a distance L_o = 8 mm from the right end of the host beam. The length from the end of the last hollow beam to the right end of the host beam is (point D) L = 30 mm.

In this example, we investigate the influence of five resonator parameters on the band gap properties of the LR beam alone. They are the resonator mass m, spring stiffness k, arm length a, and the length of the solid and hollow beam L_1 and L_2. The variation trend of the band gaps with a certain parameter is calculated by fixing the other four parameters. First, the influence of the resonator mass m on the band gaps of the LR beam is investigated by varying m from 2 to 10 g, and the other four parameters are fixed as: k= 8.1921 $\times$ 10^3 N/m, a = 10 mm, L_1 = 50 mm, and L_2 = 5 mm. As shown in Figure 10, the width of the band gap gradually increases with the resonator mass m and changes towards the lower frequency range. However, a pass band appears between the higher and lower-frequency band gaps, and the width of the pass band increases significantly with the resonator mass m. To study the effect of the spring stiffness k of the resonator on the width and frequency range of the band gaps of the LR beam, the band gaps corresponding to the variation of the spring stiffness from 2000 to 12,000 are calculated and are shown in Figure 11. The other four resonator parameters are: m = 2.0135 g, a = 10 mm, L_1 = 50 mm, and L_2 = 5 mm. It can be seen from Figure 11 that the width of the band gaps increases slightly with the spring stiffness k, and the band gaps move significantly to the higher frequency range.

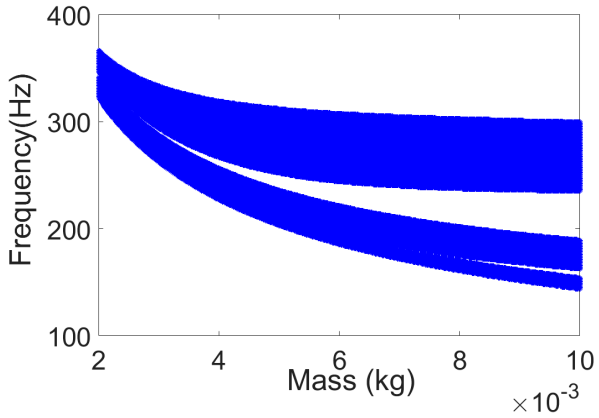

Figure 10. The width and frequency range of the band gaps vary with the resonator mass m.

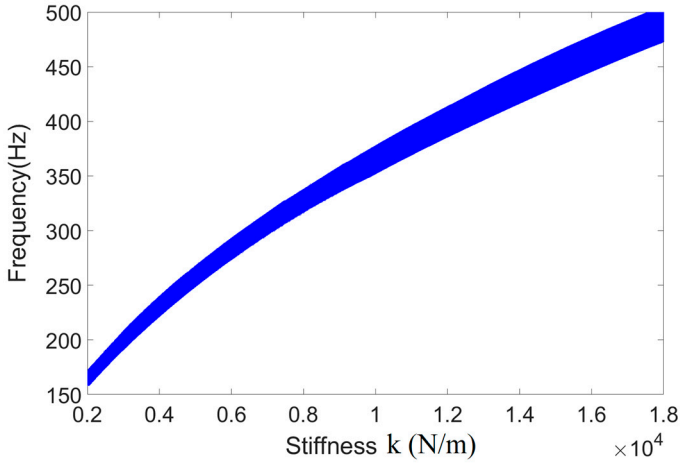

Figure 11. The width and frequency range of the band gaps vary with the spring stiffness k.

In addition, the influence of the three length parameters a, L_1, and L_2 of the resonator on the band gaps of the LR beam are also studied. Figure 12 shows the variation trend of the band gaps with the arm length a, where the other four parameters are fixed as: m = 2.0135 g, k = 8.1921 × 10^3 N/m, L_1 = 50 mm, and L_2 = 5 mm. It can be seen from Figure 12 that the width of the band gap of the LR beam increases slightly with the arm length a, and the frequency range remains nearly unchanged, thus illustrating the small effect of the arm length a on the band gaps of the LR beam. Similarly, the separate effects of the other two length parameters L_1 and L_2 on the band gaps of the LR beam are shown in Figures 13 and 14, respectively. The range of L_1 varies from 50 to 100 mm and L_2 varies from 1 to 10 mm. From Figure 13, we can see that the width of the band gap decreases with the increase in the length of L_1, and Figure 14 shows that the width of both the first and second band gaps decreases with the increase in L_2.

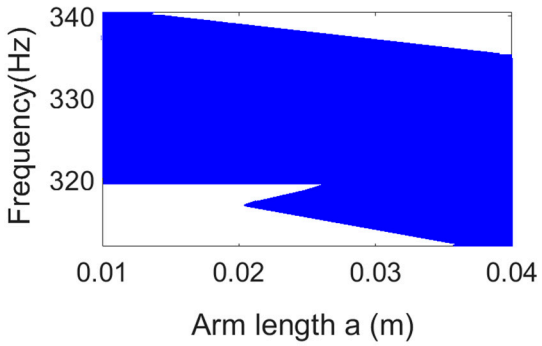

Figure 12. The width and frequency range of the band gaps vary with the arm length a.

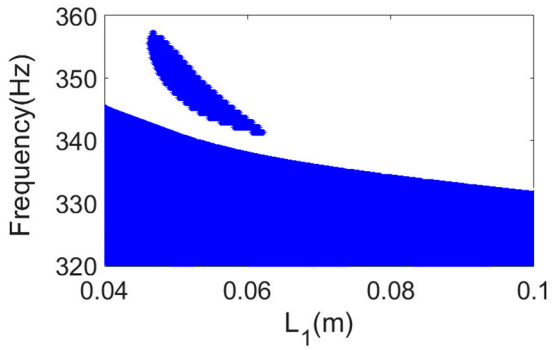

Figure 13. The width and frequency range of the band gaps vary with the arm length L_1.

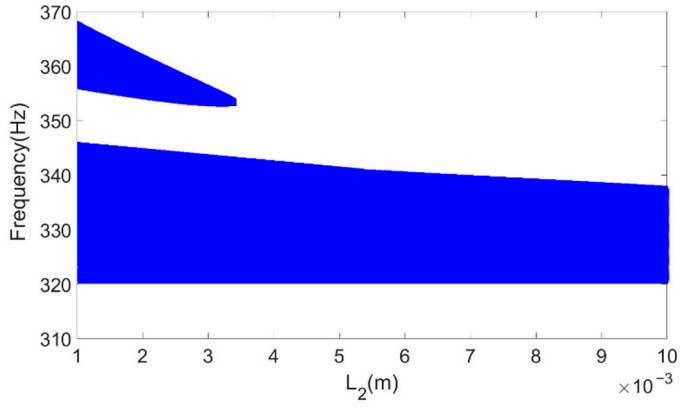

Figure 14. The width and frequency range of the band gaps vary with the arm length L_2.

Overall, the location of the band gaps of the proposed LR beam is determined by the stiffness of the spring and the mass of the resonator. Meanwhile, the width of the band gaps is related more to the mass of the resonator.

To verify the accuracy of the wave-based method, the frequency response functions (FRF) of the LR beams with two different resonators are analyzed using the wave-based approach and FEM, respectively. Both of the resonators are selected to have the same natural frequency, where the mass m and stiffness k of resonator 1 are half that of resonator 2. The natural frequency and physical parameters of the two resonators are listed in Table 1.

Table 1. Different mass and spring stiffness values of the resonator samples.

Resonator	m (g)	k (N/m)	Mode 1 (Hz)
Resonator 1	2.0135	8.1921×10^3	321
Resonator 2	4.027	1.63842×10^4	321

The FEM simulation is carried out using the ANSYS Workbench software. In the simulation, the two ends of the beam are free supported. Figure 15 shows the geometrical FEM simulation. In the simulation, the element size is set as default, and the average surface area is 9.2129×10^{-4} m^2. The element type is SOILD187. The number of total elements is 1836. The order of the accuracy of the numerical scheme is 1×10^{-4}. The red arrow depicts the harmonic force excitation applied vertically on the beam at the point with a distance L_{11} = 8 mm from the left end of the host beam. The frequency range of the excitation is from 50 to 500 Hz with a step of 2 Hz. The measured point is set with a distance L_o = 8 mm from the right end of the host beam.

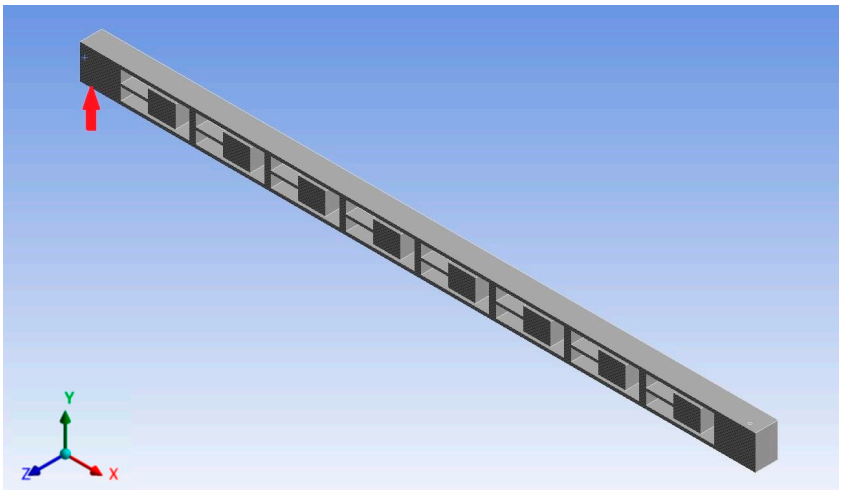

Figure 15. Structure model in the FEM simulation (cross-section drawn in the *X*-*Y* plane).

Figure 16 plots the FRFs of the LR beam suspended with resonator 1 inside, and Figure 17 shows the FRFs of the LR beam with resonator 2. As shown in Figures 16 and 17, the FRF curves calculated by the proposed wave-based method and FEM have very strong consistency, thus verifying the high accuracy of the wave-based method.

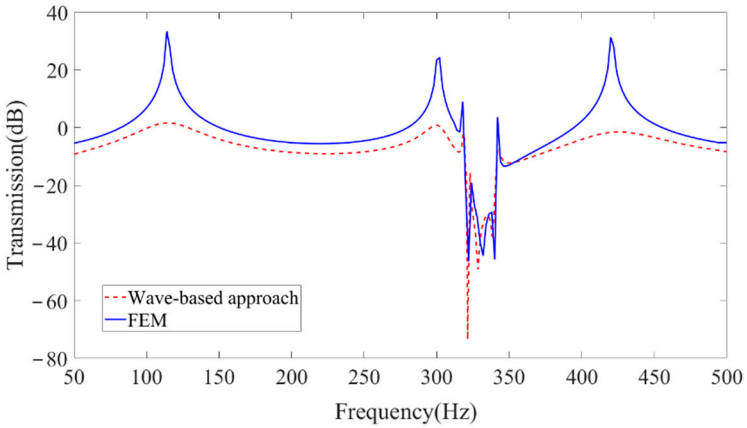

Figure 16. The FRFs of the LR beam suspended with resonator 1 using the wave-based method and FEM.

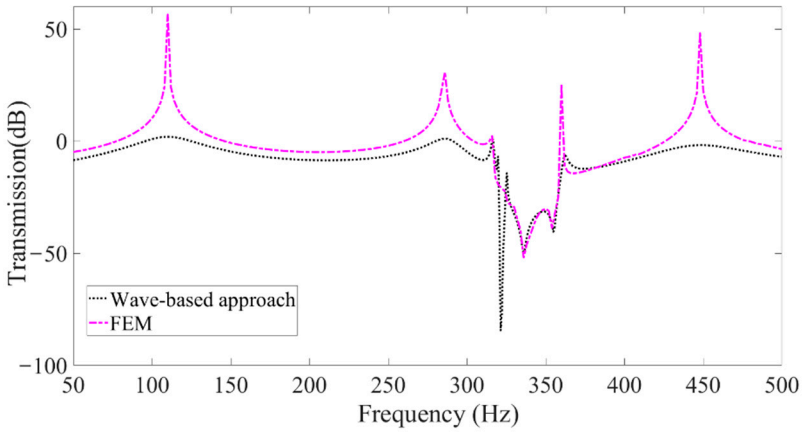

Figure 17. The FRFs of the LR beam suspended with **resonator** 2 using the wave-based method and FEM.

To further investigate the effect of the resonator on the band gaps of the designed LR beam, the FRF curves of the LR beam with two resonators are compared in Figure 18. As shown in Figure 18, the starting frequency of the band gaps of the LR beam with resonator 1 and 2 is the same. However, the width of the band gap of the LR beam with resonator 2 is 85.6% wider than that of the LR beam with resonator 1, thus demonstrating that increasing the resonator mass and spring stiffness can significantly improve the band gap width and increase the band gap center frequency of the LR beam.

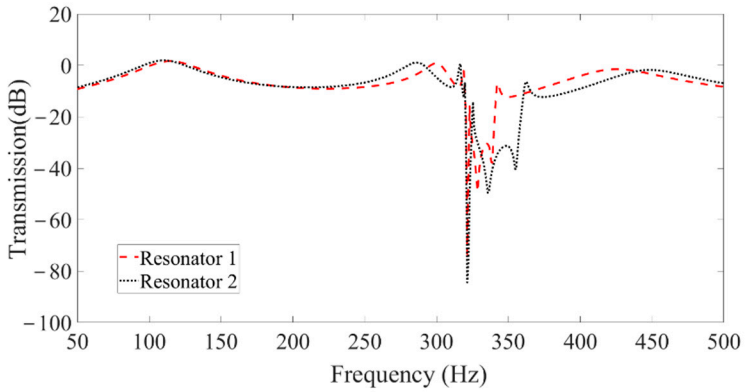

Figure 18. The FRFs of the LR **beam** suspended with different resonators.

5. Concluding Remarks

In this paper, the wave-based vibration analysis approach was employed and developed to analyze the forced vibrations of a finite lightweight LR beam suspended periodically with 2-DOF force-moment-type resonators inside. The applied force of the resonator was considered to generate waves into the host beam. The reflection and transmission matrices at the points the resonator attached were derived, and at the points of the section of the beam. Then, the propagation characteristics of the finite lightweight LR beam suspended with eight 2-DOF force-moment-type resonators were analyzed. Due to the advantage of the wave-based approach, the vibration analysis procedure was only a simple assembly of the involved reflection and transmission matrices. This approach showed the high efficiency of the derived analytical method in vibration analysis of finite LR beams. The high accuracy of the developed wave-based approach was then validated with two examples through comparison with the results obtained by FEM. Thus, the developed wave-based analysis approach was verified as a valuable tool in design and vibration analysis of finite lightweight LR beams. Moreover, the influence of the main parameters of the designed LR beam on the band gap properties was investigated. It was found that the mass and spring stiffness m and k of the resonator influenced the width and center frequency of the band gap while the length of arm a, and the length of the solid and hollow beam L_1 and L_2 barely had an influence on the band gap properties of the proposed LR beam. The results in this paper offer guidance in the design and analysis of a structure formed by lightweight LR beams, especially for vibration attenuation in a situation requiring lightweight properties, such as the space-arm and framework of antennas in the field of aerospace.

The resonator investigated in this paper was a linear type. To achieve broader band gaps, the design and analysis of an LR beam with non-linear type resonators is our future interest.

Author Contributions: Conceptualization and methodology, H.L.; writing—original draft preparation, S.L. and H.L.; Writing–review and editing, X.H. and Z.Y. All authors have read and agreed to the published version of the manuscript.

Funding: This research was supported by the National Natural Science Foundation of China (Grant No. 12102088 and 51975110), Liaoning Revitalization Talents Program (Grant No. XLYC1907171) and Fundamental Research Funds for the Central Universities (Grant No. N2003005).

Data Availability Statement: Not applicable.

Conflicts of Interest: The authors declare no conflict of interest.

References

1. Mei, C.; Li, L.; Tang, H.; Han, X.; Wang, X.; Hu, Y. Broadening band gaps of shear horizontal waves of metamaterials via graded hierarchical architectures. *Compos. Struct.* **2021**, *271*, 114118. [CrossRef]
2. Zhang, G.; Gao, Y. Topological design and magnetic tunability of a novel cross-like holes phononic crystal with low frequency. *Mech. Adv. Mater. Struc.* **2021**, 1–10. [CrossRef]
3. Stein, A.; Nouh, M.; Singh, T. Widening, transition and coalescence of local resonance band gaps in multi-resonator acoustic metamaterials: From unit cells to finite chains. *J. Sound Vib.* **2022**, *523*, 116716. [CrossRef]
4. Yu, D.; Liu, Y.; Zhao, H.; Wang, G.; Qiu, J. Flexural vibration band gaps in Euler-Bernoulli beams with locally resonant structures with two degrees of freedom. *Phys. Rev. B* **2006**, *73*, 64301. [CrossRef]
5. Zhu, R.; Liu, X.; Hu, G.; Sun, C.; Huang, G. A chiral elastic metamaterial beam for broadband vibration suppression. *J. Sound Vib.* **2014**, *333*, 2759–2773. [CrossRef]
6. Zuo, S.; Ni, T.; Wu, X.; Fan, J. Studies of band gaps in flexural vibrations of a locally resonant beam with novel multi-oscillator configuration. *J. Vib. Control* **2017**, *23*, 1663–1674. [CrossRef]
7. Zhao, P.; Zhang, K.; Deng, Z. Size effects on the band gap of flexural wave propagation in one-dimensional periodic micro-beams. *Compos. Struct.* **2021**, *271*, 114162. [CrossRef]
8. Wang, Y.; Yang, J.; Chen, Z.; Gong, X.; Du, H.; Zhang, S.; Sun, S. Investigation of a novel MRE metamaterial sandwich beam with real-time tunable band gap characteristics. *J. Sound Vib.* **2022**, *527*, 116870. [CrossRef]
9. Mohamed, R.A.; Abbas, I.A.; Abo-Dahab, S.M. Finite element analysis of hydromagnetic flow and heat transfer of a heat generation fluid over a surface embedded in a non-Darcian porous medium in the presence of chemical reaction. *Commun. Nonlinear Sci. Numer. Simula.* **2009**, *14*, 1385–1395. [CrossRef]

10. Abo-Dahab, S.M.; Abbas, I.A. LS model on thermal shock problem of generalized magneto-thermoelasticity for an infinitely long annular cylinder with variable thermal conductivity. *Appl. Math. Model.* **2011**, *35*, 3759–3768. [CrossRef]
11. Ali, L.; Liu, X.; Ali, B.; Mujeed, S.; Abdal, S.; Mutahir, A. The impact of nanoparticles due to applied magnetic dipole in micropolar fluid flow using the finite element method. *Symmetry* **2020**, *12*, 520. [CrossRef]
12. Sun, S.; Zhou, M.; Lu, W.; Davarpanah, A. Application of symmetry law in numerical modeling of hydraulic fracturing by finite element method. *Symmetry* **2020**, *12*, 1122. [CrossRef]
13. Marin, M.; Hobiny, A.; Abbas, I. The effects of fractional time derivatives in porothermoelastic materials using finite element method. *Mathematics* **2021**, *9*, 1606. [CrossRef]
14. He, M.; Ding, Q. Dynamics analysis and design of metamaterial beams with multiple half-sine waves. *Appl. Acoust.* **2022**, *186*, 108448. [CrossRef]
15. Wang, T.; Sheng, M.; Qin, Q. Multi-flexural band gaps in an Euler–Bernoulli beam with lateral local resonators. *Phys. Lett. A* **2016**, *380*, 525–529. [CrossRef]
16. Liu, Y.; Yu, D.; Li, L.; Zhao, H.; Wen, J.; Wen, X. Design guidelines for flexural wave attenuation of slender beams with local resonators. *Phys. Lett. A* **2007**, *362*, 344–347. [CrossRef]
17. Liu, L.; Hussein, M.I. Wave motion in periodic flexural beams and characterization of the transition between Bragg scattering and local resonance. *J. Appl. Mech.* **2012**, *79*, 011003. [CrossRef]
18. Tan, X.; Chen, S.; Zhu, S.; Wang, B.; Xu, P.; Yao, K.; Sun, Y. Reusable metamaterial via inelastic instability for energy absorption. *Int. J. Mech. Sci.* **2019**, *155*, 509–517. [CrossRef]
19. Zhang, Y.; Tichem, M.; Keulen, F. van. A novel design of multi-stable metastructures for energy dissipation. *Mater. Des.* **2021**, *212*, 110234. [CrossRef]
20. Ren, C.; Yang, D.; Qin, H. Mechanical performance of multidirectional buckling-based negative stiffness metamaterials: An analytical and numerical study. *Materials* **2018**, *11*, 1078. [CrossRef] [PubMed]
21. Frenzel, T.; Findeisen, C.; Kadic, M.; Gumbsch, P.; Wegener, M. Tailored buckling microlattices as reusable light-weight shock absorbers. *Adv. Mater.* **2016**, *28*, 5865–5870. [CrossRef]
22. Findeisen, C.; Hohe, J.; Kadic, M.; Gumbsch, P. Characteristics of mechanical metamaterials based on buckling elements. *J. Mech. Phys. Solids* **2017**, *102*, 151–164. [CrossRef]
23. Ma, H.; Wang, K.; Zhao, H.; Mu, R.; Yan, B. A reusable metastructure for tri-directional energy dissipation. *Int. J. Mech. Sci.* **2022**, *214*, 106870. [CrossRef]
24. Rafsanjani, A.; Akbarzadeh, A.; Pasini, D. Snapping mechanical metamaterials under tension. *Adv. Mater.* **2015**, *27*, 5931–5935. [CrossRef] [PubMed]
25. Mei, C.; Mace, B. Wave Reflection and Transmission in Timoshenko Beams and Wave Analysis of Timoshenko Beam Structures. *J. Vib. Acoust.* **2005**, *127*, 382–394. [CrossRef]
26. Leamy, M. Exact wave-based Bloch analysis procedure for investigating wave propagation in two-dimensional periodic lattices. *J. Sound Vib.* **2012**, *331*, 1580–1596. [CrossRef]
27. Lv, H.; Li, S.; Huang, X.; Yu, Z. Band-Gap Properties of Finite Locally Resonant Beam Suspended Periodically with Two-Degree-of-Freedom Force Type Resonators. *Crystals* **2021**, *11*, 716. [CrossRef]
28. Lv, H.; Leamy, M. Damping frame vibrations using anechoic stubs: Analysis using an exact wave-based approach. *J. Vib. Acoust.* **2021**, *143*, 051012. [CrossRef]
29. Mei, C. In-plane vibrations of classical planar frame structures—an exact wave-based analytical solution. *J. Vib. Control* **2010**, *16*, 1265–1285. [CrossRef]
30. Lv, H.; Zhang, Y. A wave-based vibration analysis of a finite Timoshenko locally resonant beam suspended with periodic uncoupled force-moment type resonators. *Crystals* **2020**, *10*, 1132. [CrossRef]
31. Graff, K.F. *Wave Motion in Elastic Solids*; Ohio State University Press: Columbus, OH, USA, 1975.
32. Hussein, M.; Leamy, M.; Ruzzene, M. Dynamics of phononic materials and structures: Historical origins, recent progress, and future outlook. *Appl. Mech. Rev.* **2014**, *66*, 040802. [CrossRef]